Nanoscale

Accepted Manuscript

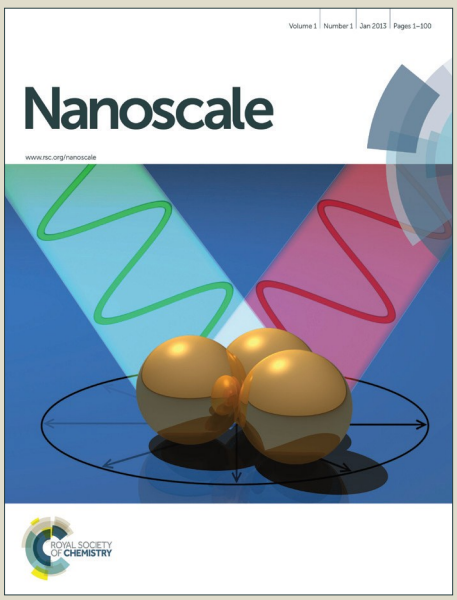

ROYAL SOCIETY OF CHEMISTRY

www.rsc.org/nanoscale

Nanoscale

ARTICLE

Thermal energy harvesting near-infrared radiation and accessing low temperatures with plasmonic sensors

Nicholas A. Karker,[a] Gnanaprakash Dharmalingam,[a] and Michael A. Carpenter[a†]

Received 00th January 20xx,
Accepted 00th January 20xx

DOI: 10.1039/x0xx00000x

www.rsc.org/nanoscale

Near-infrared (NIR) thermal energy harvesting has been demonstrated for gold nanorods (AuNRs), allowing concentration dependent, ppm-level, gas detection of H_2, CO, and NO_2 at 500°C without using a white light source. Part-per-million detection capabilities of the gold nanorods are demonstrated with a factor of 11 reduction in collection times in the NIR as compared to measurements made in the visible light region. Decreased collection times are enabled by an increase in S:N ratio, which allowed a demonstration of selectivity through the use of both full spectral and a reduced spectral-based principal component analysis. Furthermore, low temperature thermal imaging spectra have been obtained at sample temperatures ranging from 275-500°C, showing the possibility of energy harvested gas sensing at lower temperatures. These findings are promising in the area of miniaturizing plasmonic gas sensing technology and integration in areas such as gas turbines.

1 Introduction

Gas sensing at high temperatures is a challenge that has great potential in multiple industries with applications that range from optimization of combustion in power plants to sensing gas emissions from aircraft. Currently, sensitive and selective gas sensors are not stable at high temperatures and therefore cannot be placed in optimal positions to take measurements of combustion parameters. Building resilient, stable, and sensitive gas sensors that can withstand these high temperatures can save significantly on costs and reduce gas emissions.[1] Plasmonic sensors demonstrate favorable characteristics for these applications since they are stable in harsh, high temperature gas environments and have long device lifetimes. There is an abundance of literature on plasmonic gas sensing for a variety of analyte gases such as H_2, CO, NO_2 as well as organic and sulfide compounds that prove plasmonic gas sensing can potentially satisfy industry demands for high temperature, low ppm-level gas detection devices.[2-7] Plasmonic sensors utilize an optical method, which is inexpensive, and the sensors themselves are typically very small. While the plasmonically active samples are small, there is a bottleneck to implementation since, historically, plasmonic based sensing requires both external incident light sources and wavelength dispersive detectors.

The ability to harvest thermal energy from combustion sources reduces design complexity and favors practical integration schemes. Previous work has demonstrated the feasibility of such a thermal energy harvesting approach in the visible light region but suffered from the low amount of total spectral radiance in this range.[10] Previous thermal energy harvesting results required 4-8 minute spectral collection times, had low S:N at wavelengths below ~650nm, and showed no gas selectivity between reducing gases. The current work fixed these issues, resulting in collection times less than 30 seconds while simultaneously improving the S:N ratio across the spectral range. The novelty demonstrated within the current work is based on extending the energy harvesting methods into the NIR to wavelengths around 1400nm, which has led to the demonstration of wavelength down-selection while maintaining both high sensitivity and selectivity towards the target gases. Wavelength down-selection has reduced the number of wavelength variables for gas selectivity to three individual wavelengths. Thus this work has for the first time demonstrated that high quality plasmonics sensing data is achievable without both an external incident light source as well as complex detection optics. Additionally, optical sensing in the NIR has the benefit of comparatively low cost optics and electronics due to the mass usage of NIR equipment by the telecommunication industry.[8] The results detailed in this work demonstrate a clear path between proof-of-concept and a usable high temperature, high response gas sensor that can be used in combustion environments.

In order to sufficiently harvest thermal radiation from the NIR regime, 44x170nm gold nanorods (AuNRs) have been fabricated due to the strong longitudinal peak position dependence on the aspect ratio (rod length divided by rod width).[9] AuNR samples, with their longitudinal peak in the near-infrared region, will be shown to offer rapid gas sensing capabilities without an external incident white light source. Gas selectivity has also been shown by monitoring several key wavelengths within the plasmonic absorption band. These features allow miniaturization of typically large sensing

[a] SUNY Polytechnic Institute, Colleges of Nanoscale Science and Engineering, 257 Fuller Road, Albany, New York 12203, United States
† Corresponding author email: mcarpenter@sunycnse.com

components. Another benefit of thermal harvesting in the NIR is that the sensors can operate at a broader temperature range. In the current study, low temperature thermal imaging spectra have been collected down to a sample temperature of 275°C. Further use of these methods should be widely applicable to plasmonics related work in energy, biological and other materials related fields with operating temperatures ranging from ambient conditions up to those applicable to combustion, simply by tuning the aspect ratio of the plasmonic absorber to best match the thermal conditions. This technique should also allow extraction of sample temperature due to the demonstrated linear increase of plasmon peak position with increasing temperature. Alternatively, by using a selected wavelength approach that tracks independent wavelengths for both temperature and gas concentration, temperature extraction as well as analyte gas selectivity could be possible within a single AuNR sample.

Plasmonic sensors utilize the properties of a surface plasmon resonance (SPR), created by incident light exciting conduction band electron oscillations, which induces the scattering and absorption of light. When the interrogated particles are smaller than the wavelength of the incident light, a localized surface plasmon resonance (LSPR) occurs, which refers to the confinement of the electron oscillations to the particle surface. LSPR results in a localized electromagnetic field enhancement that is strongly sensitive to the dielectric constant of the local environment immediately surrounding the nanoparticle, thereby allowing sensitive gas detection since even small amounts of adsorbed/reacted analyte gas is enough to alter the matrix dielectric constant and the metal's free electron density.

Lithographically patterned AuNRs offer several advantages that make them the focus of this work. Patterned AuNRs have benefits of uniformity of the rod size and spacings as well as ease of tunability. Additionally, patterned AuNRs with a YSZ capping layer have been shown to be thermally stable at the high temperatures and reactive conditions common in combustion environments.[12] The thermal stability of AuNRs with a YSZ capping layer has been further reinforced by multiple 20 hour gas sensing experiments with both white lightand thermal imaging measurements on the same nanorod sample.[10] The benefits of YSZ-capped, lithographically patterned AuNRs make them an ideal candidate for tests that harvest NIR radiation from combustion sources.

For spherical nanoparticles, the LSPR frequency is expressed by the Drude equation, which relates it to the free electron density of the metal nanoparticle and the matrix dielectric constant. Shape-dependent SPR properties such as those present in AuNRs can be modeled by modifying the Drude equation with a shape factor, Y_i, which accounts for the effects of the nanorod aspect ratio.

$$\omega = \sqrt{\frac{N_0 e^2}{(\varepsilon_b + Y_i \varepsilon_m) m_e \varepsilon_0}}$$

Equation 1. Drude equation for determining the resonant peak frequency (ω) of nanorods. N_0 is the free electron density, e is the elementary charge, ε_b is the interband transition term, ε_m is the dielectric constant of the matrix, Y_i is the shape factor for the i^{th} axis, m_e is the mass of an electron, and ε_0 is the free space permittivity.

The resonant peak frequency of AuNRs is described by eq. 1 and is a function of the dielectric constant of the metal, dielectric constant of the matrix, and the free electron density. Different gas environments can alter these parameters and lead to different optical responses, opening the door for gas sensing. The AuNR-YSZ sample used in these high temperature sensing studies has a baseline resonant frequency in an air atmosphere, determined by molecular oxygen dissociative adsorption and formation of different ionized species with eventual formation of monoatomic oxygen anions (O^-).[13] The monoatomic oxygen anions can fill vacancy sites in the YSZ matrix after extracting another electron to form O^{2-}. The different analyte gases used in this study also adsorb to the sample surface and either donate or remove oxygen anions from the YSZ matrix, affecting the free electron density of the metal and the matrix dielectric constant. A plasmon peak shift to higher energies is caused by reducing gases, H_2 or CO, where surface adsorption and subsequent reaction with an oxygen anion forms H_2O and CO_2, respectively. These reactions consequently increase the free electron density and decrease the matrix dielectric constant causing a blue shift in the LSPR peak position. A peak shift to lower energies occurs upon exposure to an oxidizing gas such as NO_2, and is due to dissociation of the NO_2 onto the sample surface and oxygen donation to the matrix causing electron transfer from the gold and an increase in the matrix dielectric function. By collecting frequent absorbance spectra during a gas exposure experiment and extracting the longitudinal peak position from each one, the peak position can be seen to change significantly and characteristically with each analyte gas type.

2 Results and Discussion

The thermal radiation emitted by a high temperature combustion source is isotropic but, through experimental design, the NIR thermal radiation can be effectively focused through the plasmonically active AuNR sample and be used as the incident light source. In this work, and as schematically shown in fig. 1, a spherical gold-coated mirror with high reflectivity in the NIR region, was used for the purpose of redirecting light exiting the furnace back through the AuNRs for enhanced spectral acquisitions. Collection optics with computer controlled mass flow controllers and a NIR spectrometer complete the hardware needed to acquire

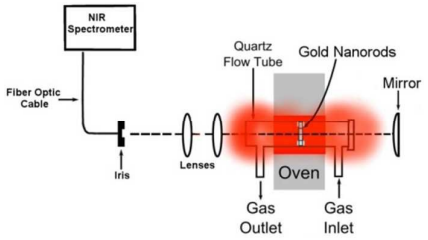

Figure 1. Schematic of the thermal imaging bench setup.

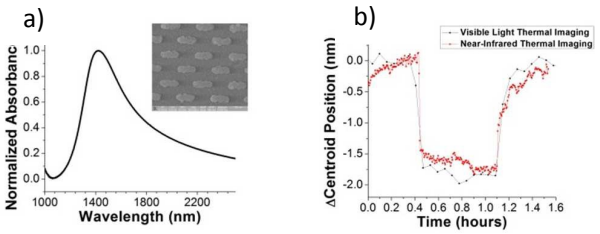

Figure 2. (a) Room temperature FTIR spectra showing the longitudinal NIR plasmon peak of the 44x170nm Au nanorod sample and inset eSEM image of the 44x170nm AuNR-YSZ sample and (b) comparison of data point frequency for visible light-absorbing AuNR sample (spectrum collection time = 220 seconds) and NIR-absorbing AuNR sample (spectrum collection time = 20 seconds). The starts of the 10000 ppm H_2 exposures from both tests were set to t=0 hours for comparison. Each data point averages 10 spectra.

energy harvested NIR absorption spectra referenced to the thermal radiation emitted by the furnace.

To allow for thermal energy harvesting of near-infrared radiation, rods with dimensions of 44x170nm were fabricated for this study, which resulted in a longitudinal plasmon peak position of approximately 1420nm (fig. 2a) which is ideal for NIR energy harvesting.

Referencing Planck's blackbody distribution curve, it is clear there is a significant increase in spectral radiance in the near infrared region as compared to the visible region at the same temperature. For a blackbody emitter temperature of 600°C, the spectral radiance at 1420nm is 458x higher than the spectral radiance emitted at 800nm. While this calculation is for an ideal blackbody, this is qualitatively apparent in the experimental data noted in fig. 2b. Specifically, with these higher signal counts in the NIR, 11x more data points were able to be collected within a given gas exposure experiment, thus enabling improved spectral and time dynamic data sets.

A single NIRQuest512 near-infrared spectrometer was used to measure NIR absorbance spectra as a function of both time and gas exposures for these sensing experiments. A mathematical replacement for a real-time reference was used to achieve improved baseline stability. Specifically, a method known as internal referencing was used to correct for baseline drift.[14,15] Internal referencing requires selection of a single non-absorbing wavelength for a given sample and then using that wavelength to "re-normalize" the rest of the absorbance curve to the absorbance value at that wavelength. All optical sensing experiments, especially those at long time scales, benefit from having a real-time reference since light sources always have varying scan-to-scan intensity across the spectral range and also drift systematically. A technique such as internal referencing is a solution to this problem and can also work with the thermal harvesting technique since, similar to white light experiments, the intensity of thermal radiation produced by the furnace coils varies slightly around the furnace setpoint. This typically is not a significant problem in the thermal harvesting experiments, but provides extra stabilization to the technique over the 20 hour gas exposure experiments.

Gas sensing using the internal referencing procedure has been performed for different levels of H_2, CO, and NO_2 exposures up to maximum concentrations of 10000 ppm H_2, 100 ppm CO, and 100 ppm NO_2 in an air background and a 500°C sample temperature. The purge time for each analyte gas concentration in all of the sensing tests was 40 minutes. The absorption spectral data acquired from these experiments were used to determine the change in the LSPR centroid position as a function of time and gas exposure, Figure 3 (top), as well as the calibration curves determined from these exposures, Figure 3 (bottom). As expected both the H_2 and CO exposures show a characteristic blue shift in the LSPR while NO_2 exposures result in a red shift in the LSPR.

The calibration curves shown in fig. 3 were made by averaging 25 centroid positions from each gas concentration and then plotting this averaged centroid shift vs. gas concentration for the three analyte gases. The average error

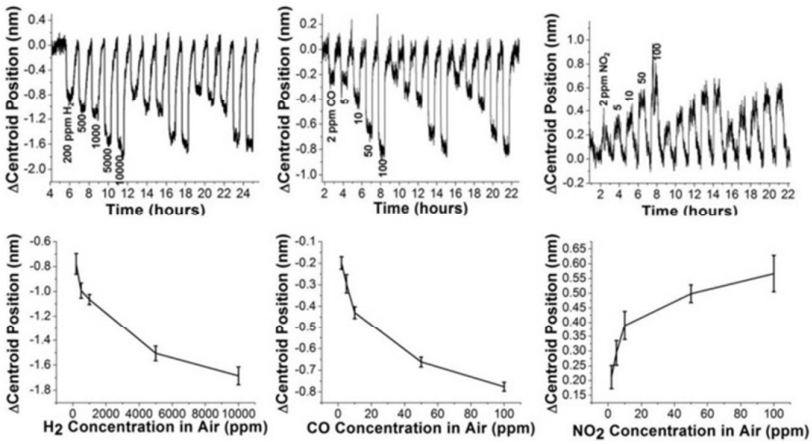

Figure 3. (Top Row) Gas sensing for the analyte gases: H_2, CO, and NO_2. (left) 200, 500, 1000, 5000, and 10000 ppm H_2 in air carrier gas. (middle) 2, 5, 10, 50, 100 ppm CO in air carrier gas. (right) 2, 5, 10, 50, 100 ppm NO_2 in air carrier gas. A spectral smoothing procedure was done followed by internal referencing to minimize baseline drift. The remaining baseline drift was corrected by removing linear drifts of 0.6 nm from the H_2 curve, 0.65 nm from the CO curve, and 0.5 nm from the NO_2 curve. The centroid position, or the center of mass of the absorbance curve, was used to track changes in the LSPR peak position.
(Bottom Row) Calibration plots for the H_2, CO, and NO_2 results shown in top row. Each data point averages 25 individual centroid positions from the Δcentroid vs. time graph to determine the average shift at each analyte gas concentration.

bar percentages are 5.7% for H_2, 8.3% for CO, and 12.5% for NO_2. In all of the tests, the observed baseline noise is translated to the analyte gas response since it is noise coming from the detector as well as the light source. In the NO_2 test, since it has the smallest magnitude of peak shift between the three gases, the noise is more prevalent in the gas response and this is seen from the high error bar percentage. All of the calibration curves shown appear to have not reached their saturation limit, and could likely give concentration dependent measurements at higher concentrations of the analyte gases. Lower limit sensitivity values for the three analyte gases are: -0.00034 nm/ppm H_2, -0.029 nm/ppm CO and 0.022 nm/ppm NO_2 and were calculated by analyzing the slopes of the calibration curves for the lowest three concentrations for each analyte gas. Lower concentrations of NO_2 and CO were used to illustrate the high sensitivity at concentrations important to industrial applications. Specifically, a study by General Electric reports that a stationary gas turbine has between 2-20 ppm NO_2 and between 5-330 ppm CO by volume in its exhaust stream,[16] which fall within the detection capabilities of the sample used here. These results demonstrate the concentration dependence and sensitivity achievable with the thermal imaging method. However, distinguishing the analyte gas responses, especially the two reducing gases, remains a concern. One approach to addressing this problem is Principal Component Analysis (PCA). PCA is a popular multivariate analysis method that is used in fields such as image compression,[17] electronic noses,[18,19] and gas sensing[20-22] to visualize seemingly hidden relationships between independent variables.

PCA has been performed for the H_2, CO, and NO_2 gas sensing results shown above. PCA is done by reducing the dimensionality of a vast dataset, through Singular Value Decomposition (SVD), by projecting the data points onto the eigenvectors of the covariance matrix which correspond to the principal component axes or the directions of maximum variance within the data. This results in a PCA scores plot which can show clustering of data representing each gas. For these measurements, the inputs to the PCA algorithm are averaged difference spectra (i.e. air-H_2 spectra minus the air-only spectra) for the 5 different concentrations. Figure 4a shows the full spectrum PCA result that contains 413 wavelengths in the range of 1050nm-1700nm. Similar degrees of selectivity are achieved with the reduced wavelength approach (fig. 4b) by selecting the wavelengths: 1350, 1410, 1470nm. The wavelengths 1350 and 1470nm were selected to capture variance on either side of the LSPR absorbance peak, where the intensity at a given wavelength is shifting a particularly large amount from either a red or blue curve shift. The 1410nm wavelength was chosen due to its proximity to the plasmon peak position. Comparison of the gas-on and gas-off spectral overlays confirmed the choice of this wavelength subset. By reducing the wavelengths collected, we can reduce the amount of collected information significantly. By only requiring a small subset of wavelengths to be monitored while retaining the required detection limits and selectivity characteristics, the detection hardware can be simplified. NIR optical components such as sources and spectrometers already have low cost and are highly available due to demand from the telecommunications industry.[8,23] AuNR-YSZ samples could be mounted on fiber optic cables and, combined with wavelength-dispersive multiplexing and detectors, would allow placement of a distributed network of optical plasmonic sensors in a combustion source. The NIR thermal energy harvesting approach along with multivariate analysis opens a pathway for miniaturization and integration of low-cost optical gas sensors.

The NIR thermal energy harvesting method can also function at lower temperature regimes. Lower temperatures are of great appeal as applications such as photothermal therapy or bio-imaging, or combustion/catalytic environment applications would benefit from sensors that harvest low temperature thermal radiation. Using catalysts at lower temperatures allow improved energy efficiency and increased long-term stability of the catalyst. Previous work illustrates that most current catalysts rely solely on high temperatures to surpass activation barriers. To address the high temperature constraint, the Linic group, has developed Ag plasmonic nanostructures that allow low temperature catalysis which utilize a combination of sample heating and low-intensity visible light to drive catalysis.[24] By demonstrating that low temperature thermal imaging spectra can be collected, it is possible the AuNR sample could act in a similar fashion, but would instead harvest and use the thermal radiation to reduce complexity.

Fig. 5 shows that the longitudinal peak position of the NIR-absorbing AuNR sample increases linearly with temperature for polarized white light measurements. Thermal imaging spectra have been taken at a series of similar sample temperatures and extend down to a sample temperature of ~275°C (the lowest temperature thermal imaging spectra is shown inset in fig. 5). There are several spectral features that

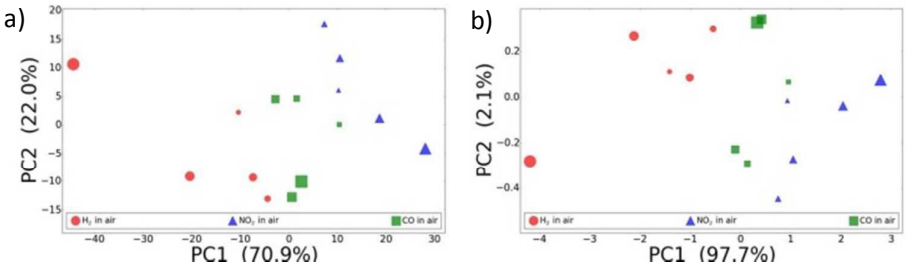

Figure 4. (a) Full spectrum PCA performed on wavelength range of 1050nm-1700nm. (b) Reduced wavelength PCA using wavelengths of 1350, 1410, 1470nm with similar selectivity as with the full spectrum PCA.

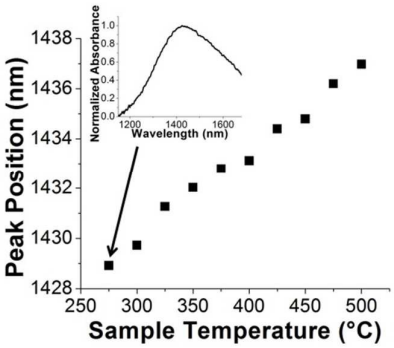

Figure 5. Plot showing increase of peak position with sample temperature for horizontally polarized white light measurements. Thermal imaging spectra have been collected at similar temperatures down to a sample temperature of 275°C which is shown as an inset graph.

are expected to change with temperature. First, the full width at half maximum increases with increasing temperatures due to electron-phonon scattering. Also, due to thermal expansion of the particles, the free electron density will decrease due to the same number of free electrons occupying a larger volume.[11]

The linear peak position dependence on sample temperature for the white light measurements points to the possibility of temperature extraction with both white light as well as thermal imaging measurements, though additional work will be required to demonstrate reliable temperature extraction with thermal imaging. In theory, the plasmon linewidth (FWHM) should allow temperature extraction due to the temperature dependence of linewidth as demonstrated with spheroidal metal particles.[25] Another approach for simultaneous temperature sensing is to find a wavelength that is active only with changes in temperature and not affected by the presence of gases.[11] Based on the current gas reaction mechanism as described above, it is likely that this nanorod sample could still work for gas sensing down to a sample temperature of ~350°C since YSZ continues to conduct oxygen ions down to this temperature. There is a temperature threshold (typically below ~350°C) for the YSZ matrix where oxygen ion conduction becomes less appreciable and it may be beneficial to instead use TiO_2, CeO_2 or another active material to obtain gas sensing measurements.

3 Conclusions and Future Directions

Industrial applications desire increased signal for optical sensing measurements as this permits faster gas detection and an increased signal-to-noise ratio. In this work, it is shown that thermal energy harvesting methods can be extended into the near-infrared region by demonstrating concentration dependent surface plasmon peak shifts and gas selectivity with both full spectrum PCA analysis and reduced wavelength PCA analysis. These advances could potentially reduce the required white light source to a mirror and the full-size spectrometer down to a handful of wavelength-tuned diode detectors to monitor selected highly information-dense wavelengths and collect both sample and reference measurements for a given wavelength.

There are several exciting avenues for future work built on top of these results. Rods could be fabricated that absorb in the mid-infrared, allowing even lower temperature thermal imaging spectra to be obtained. The thermal imaging method could be pushed to potentially allow absorption measurements down to body temperature and give *in vivo* sensing measurements. This could allow photothermal therapy or bio-imaging with these particles all using surface plasmon resonance. NIR absorbing gold nanoparticles have already been shown to be viable candidates for the next generation of advances in photothermal therapy as well as imaging due to low cytotoxicity, biocompatibility, and deep tissue penetration of NIR radiation.[26,27] It is known that such long rods are efficient light scatterers so there is a balancing act between the absorption and scattering pathways and the greatest potential may actually lie in using NIR absorbing rods for bio-imaging.[28]

4 Methods

Nanorod sample preparation

The 44x170 nm nanorod sample used in this study was fabricated in the same way as shown previously and uses both physical vapor deposition and electron-beam lithography.[12] A 65nm YSZ base layer was used, on top of which the AuNRs were lithographically patterned. This was followed by the deposition of a "capping" layer of YSZ of 50nm thickness. A step anneal process was then used on the nanorod sample at temperatures of 300, 400, 500, and 600°C.

Gas Sensing

A NIRQUEST 512 element array detector was used that provided a spectral range of 900-1700nm allowing near infrared absorption measurements. The parameters for the collected spectra were 2 second integration time per scan and 10 scans were averaged for one spectra.

Acknowledgements

This work was supported by the United States Department of Energy National Energy Technology Laboratory under contract number DE-FE0007190. Any opinions, findings, and conclusions or recommendations expressed in this publication are those of the authors and do not necessarily reflect the views of the United States Department of Energy National Energy Technology Laboratory.

References

1 S. Akbar, P. Dutta, C. Lee, High-temperature ceramic gas sensors: A review, Int. J. Appl. Ceram. Tec., 2006, **3**, 302-311.

2 P. Rogers, G. Sirinakis, M. A. Carpenter, Plasmonic-Based Detection of NO_2 in a Harsh Environment, J. Phys. Chem. C, 2008, **112**, 8784-8790.
3 G. Sirinakis, R. Siddique, I. Manning, P. Rogers, M. A. Carpenter, Development and Characterization of Au-YSZ Surface Plasmon Resonance Based Sensing Materials: High Temperature Detection of CO, J. Phys. Chem. B, 2006, **110**, 13508-13511.
4 P. Rogers, G. Sirinakis, M. A. Carpenter, Direct Observations of Electrochemical Reactions Within Au-YSZ Thin Films via Absorption Shifts in the an Nanoparticle Surface Plasmon Resonance, J. Phys. Chem. C, 2008, **112**, 6749-6757.
5 P. R. Ohodnicki, T. D. Brown, G. R. Holcomb, J. Tylczak, A. M. Schultz, J. P. Baltrus, High temperature optical sensing of gas and temperature using Au-nanoparticle incorporated oxides. Sens. Actuators, B, 2014, **202**, 489-499.
6 E. Della Gaspera, A. Mura, E. Menin, M. Guglielmi, A. Martucci, Reducing gases and VOCs optical sensing using surface plasmon spectroscopy of porous TiO_2-Au colloidal films, Sens. Actuators, B, 2013, **187**, 363-370.
7 E. Della Gaspera, M. Pujatti, M. Guglielmi, M. Post, A. Martucci, Structural Evolution and Hydrogen Sulfide Sensing Properties of $NiTiO_3$-TiO_2 Sol-Gel Thin Films containing Au Nanoparticles, Mater. Sci. Eng. B - Adv., 2011, **176**, 716-722.
8 K. J. Kim, X. Y. Chong, P. B. Kreider, G. H. Ma, P. R. Ohodnicki, J. P. Baltrus, A. X. Wang, C. H. Chang, Plasmonics-enhanced metal-organic framework nanoporous films for highly sensitive near-infrared absorption, J. Mater. Chem. C, 2015, **3**, 2763-2767.
9 J. Perez-Juste, I. Pastoriza-Santos, L. Liz-Marzan, P. Mulvaney, Gold Nanorods: Synthesis, Characterization and Applications, Coord. Chem. Rev., 2005, **249**, 1870-1901.
10 N. Karker, G. Dharmalingam, M. A. Carpenter, Thermal Energy Harvesting Plasmonic Based Chemical Sensors, ACS Nano, 2014, **8**, 10953-10962.
11 P. R. Ohodnicki, M. P. Buric, T. D. Brown, C. Matranga, C. J. Wang, J. Baltrus, M. Andio, Plasmonic Nanocomposite Thin Film Enabled Fiber Optic Sensors for Simultaneous Gas and Temperature Sensing at Extreme Temperatures, Nanoscale, 2013, **5**, 9030-9039.
12 N. A. Joy, B. K. Janiszewski, S. Novak, T. W. Johnson, S. H. Oh, A. Raghunathan, J. Hartley, M. A. Carpenter, Thermal Stability of Gold Nanorods for High-Temperature Plasmonic Sensing, J. Phys. Chem. C, 2013, **117**, 11718-11724.
13 X. Xia, R. J. Oldman, C. R. A. Catlow, Oxygen adsorption and dissociation on yttria stabilized zirconia surfaces, J. Mater. Chem., 2012, **22**, 8594-8612.
14 M. A. Eddings, J. W. Eckman, C. A. Arana, G. A. Papalia, J. E. Connolly, B. K. Gale, D. G. Myszka, "Spot and hop": Internal referencing for surface plasmon resonance imaging using a three-dimensional microfluidic flow cell array, Anal. Biochem., 2009, **385**, 309-313.
15 C. Zhou, Y. Mu, M. C. Yang, Q. Song, Y. Zhang, Z. Y. Wu, L. C. Xiang, W. Jin, Q. H. Jin, A gravity-induced flow injection system for surface plasmon resonance biosensor, Talanta 2013, **112**, 95-100.
16 R. Pavri, G. Moore, Gas turbine emissions and control, GE Power Systems, 2001.
17 R. d. E. Santo, Principal Component Analysis applied to digital image compression, Einstein (São Paulo), 2012, **10**, 135-139.
18 A. H. Gomez, J. Wang, G. X. Hu, A. G. Pereira, Electronic nose technique potential monitoring mandarin maturity, Sens. Actuators, B - Chem., 2006, **113**, 347-353.
19 S. Gupta, P. S. Variyar, A. Sharma, Application of mass spectrometry based electronic nose and chemometrics for fingerprinting radiation treatment, Radiat. Phys. Chem., 2015, **106**, 348-354.
20 A. A. Tomchenko, G. P. Harmer, B. T. Marquis, J. W. Allen, Semiconducting metal oxide sensor array for the selective detection of combustion gases, Sens. Actuators, B - Chem., 2003, **93**, 126-134.
21 Y. J. Lu, C. Partridge, M. Meyyappan, J. Li, A carbon nanotube sensor array for sensitive gas discrimination using principal component analysis, J. Electroanal. Chem., 2006, **593**, 105-110.
22 N. A. Joy, M. I. Nandasiri, P. H. Rogers, W. L. Jiang, T. Varga, S. Kuchibhatla, S. Thevuthasan, M. A. Carpenter, Selective Plasmonic Gas Sensing: H_2, NO_2, and CO Spectral Discrimination by a Single Au-CeO_2 Nanocomposite Film, Anal. Chem., 2012, **84**, 5025-5034.
23 T. Lee, Development of integrated semiconductor optical sensors for functional brain imaging, UMI Dissertations Publishing, 2008.
24 P. Christopher, H. L. Xin, S. Linic, Visible-light-enhanced catalytic oxidation reactions on plasmonic silver nanostructures, Nature Chemistry, 2011, **3**, 467-472.
25 N. I. Grigorchuk, Temperature dependence of plasmon resonances in spheroidal metal nanoparticles, Conden. Matter Phys., 2013, **16**, 18.
26 F. Jabeen, M. Najam-ul-Haq, R. Javeed, C. W. Huck, G. K. Bonn, Au-Nanomaterials as a Superior Choice for Near-Infrared Photothermal Therapy, Molecules, 2014, **19**, 20580-20593.
27 R. C. Lv, P. P. Yang, Y. L. Dai, S. L. Gai, F. He, J. Lin, Lutecium Fluoride Hollow Mesoporous Spheres with Enhanced Up-Conversion Luminescent Bioimaging and Light-Triggered Drug Release by Gold Nanocrystals, ACS Applied Materials & Interfaces, 2014, **6**, 15550-15563.
28 X. H. Huang, S. Neretina, M. A. El-Sayed, Gold Nanorods: From Synthesis and Properties to Biological and Biomedical Applications, Adv. Mater., 2009, **21**, 4880-4910.

